Barriers to transport induced by periodic oscillations in a physical model of the human vitreous chamber

Alberto Oliveri,[1] Alessandro Stocchino,[2] and Marco Storace[1,*]

[1]*Dipartimento di Ingegneria Biofisica ed Elettronica, University of Genoa, Via Opera Pia 11a, I-16145 Genoa, Italy*

[2]*Dipartimento di Ingegneria delle Costruzioni, dell'Ambiente e del Territorio, University of Genoa, Via Montallegro 1, I-16145 Genoa, Italy*

(Received 1 December 2010; published 18 March 2011)

Understanding mixing processes that occur in the human vitreous chamber is of fundamental importance due to the relevant clinical implications in drug delivery treatments of several eye conditions. In this article we rely on experimental observations (which demonstrated that dispersion coefficients largely dominate diffusive coefficients) on a physical model of the human eye to perform an analysis based on Lagrangian trajectories. In particular, we study barriers to transport in a particularly significant two-dimensional section of the eye model by using nonlinear dynamical systems theoretical and numerical tools. Bifurcations in the system dynamics are investigated by varying the main physical parameters of the problem.

DOI: 10.1103/PhysRevE.83.036311 PACS number(s): 47.63.−b, 05.45.−a, 47.51.+a, 87.85.gf

I. INTRODUCTION

The posterior chamber of the eye represents most of the volume of the human eye and is filled with vitreous humor, an incompressible, transparent, and either viscoelastic or Newtonian fluid which accomplishes several mechanical and physiological tasks [1]. The shape of the vitreous chamber is mostly spherical except for an indentation in the anterior part (due to the presence of the lens), whose size can be approximately 10%–30% of the eye globe mean radius. The human vitreous can be set in motion by different kinds of eye rotations. The main eye movements occur with a vertical axis of rotation and are usually termed as saccades. The saccades are characterized by a wide range of amplitude and duration and have several physiological causes, for example, redirecting the line of sight. Metrics of saccadic eye movements are reported in detail in Ref. [2]. In the same reference, measurements of the human eye movements are reported in different circumstances and in many cases saccadic movements possess a strong periodicity. Based on these observations, in the present analysis, saccades, as a first approximation, are reproduced with periodic sinusoidal torsional oscillations $\varepsilon(t) = A\sin(\omega t)$, where A is the oscillation amplitude and ω the angular frequency.

A potentially important clinical implication of vitreous humor dynamics is its effect on mass transport in the posterior chamber. Indeed, several eye conditions (age-related macular degeneration, glaucoma, diabetic retinopathy) are treated by intravitreal delivery of drugs using different techniques [3] and, moreover, several drugs are effective only inside a narrow range of concentrations and for a prescribed length of time [4]. Thus, an understanding of mixing processes in the vitreous humor is extremely important to obtain the desired performances of the medical treatment. In the literature many studies (theoretical and numerical) are reported regarding exclusively diffusive transport in the vitreous humor (see Ref. [5] for a comprehensive bibliography), disregarding completely the role of the vitreous motion due to saccades. On the contrary, the dynamical processes that the vitreous undergoes during typical eye movements can dramatically influence the mass transport within the vitreous chamber. Recent studies [6,7] showed experimentally and analytically that, in addition to a leading-order oscillatory flow, a Newtonian fluid undergoing torsional sinusoidal oscillations also has a steady streaming component that appears at second order and consists of two counter-rotating toroidal vortices, one in each hemisphere for a perfect sphere and in a more complicated flow pattern in a deformed domain as in the present case. The leading-order flow component is purely oscillatory, thus, it does not produce a net particle drift after each period. On the contrary, the steady streaming flow induces a particle drift over long time scales whose consequences on the mass transport have been described in Ref. [7]. The main result of the analysis in the latter study was that the dispersion coefficients are four orders of magnitude larger than the molecular diffusion coefficient. In the same reference a brief outline of the role of flow inhomogeneity, known to be relevant in mass transport [8], was given. In fact, since the mentioned study was based on Lagrangian absolute statistics, the effect of spatially distributed flow structures was by definition disregarded due to the fact that Lagrangian statistics involve averages over many particles. In particular, particles displacements near energetic structures, like vortices, are averaged together with others in quiescent regions, concealing the possibility to detect Lagrangian material structures.

The experimental measurements were conducted mainly on the equatorial plane, being a plane of symmetry for the domain, on which the flow is perfectly two-dimensional (2D). A smaller set of measurements were also conducted on the vertical plane containing the centers of both the sphere and the lens, which is in turn a plane of symmetry for the domain. Here, we present an extensive analysis of the mixing processes occurring within a physical model of the vitreous chamber during periodic oscillations, with the aim of investigating the presence of barriers to transport (also known as Lagrangian coherent structures or LCSs) and their dependence on the main physical parameters. These structures were not investigated at all in Ref. [7].

Since LCSs are, by definition, material structures of the flow, they act as barriers to mass transport, inhibiting in some

*marco.storace@unige.it

circumstances an efficient mixing; see Refs. [9–14] among many others.

II. EXPERIMENTAL SETUP

The experimental model we used for the 2D particle image velocimetry (2D-PIV) measurements [7] is sketched in Fig. 1, where the vitreous chamber is modeled as a sphere of radius R_0 with an indentation of size L on one side, representing the human lens. Typically the human eye globe radius is about 10–12 mm and the lens produces an indentation that may vary from 10% to 30% of the mean radius, depending on the age and healthiness of the subject [1]. In the same reference the characteristic value of the vitreous viscosity can be found, which can assume values ranging from 7×10^{-4} m^2 s^{-1} (healthy vitreous) down to a value similar to the water viscosity. The latter case is true when the vitreous is completely liquefied or replaced with tamponade fluids.

In the present analysis, we treat the vitreous as a Newtonian fluid and, therefore, the physical model is filled with an incompressible Newtonian fluid, namely an aqueous solutions of glycerol at concentrations between 70% and 98%. The dynamic viscosity of the working solution was measured at the beginning of each experimental run using a falling ball viscometer, and care was taken to maintain a constant room temperature during each experimental run so the viscosity remained constant.

The Eulerian flow resulting by setting in oscillation the model around the z axis is governed by three dimensionless parameters: the Womersley number $\alpha = \sqrt{R_0^2\omega/\nu}$ (where ν is the kinematic viscosity of the fluid), the torsional oscillation amplitude A, and a geometrical parameter, namely the indentation size $\delta = L/R_0$. The Womersley number can be physically interpreted as the ratio between the characteristic dimension of the domain (R_0) and the thickness of the Stokes-type boundary layer at the wall. During typical eye movements, A can take any value up to $\pi/4$, whereas the value of α may take a wide range of values spanning many orders of magnitude from order 1 up to around 10^4 in the case of microsaccades [2]. In particular, eye movements can be generated by different causes and for different tasks. Many studies have been devoted to analyze the characteristics of several kinds of eye movements, in addition to the single saccades. For example, the eye globe movements during reading have been extensively studied by the authors of Refs. [15,16] and they found that, on average,

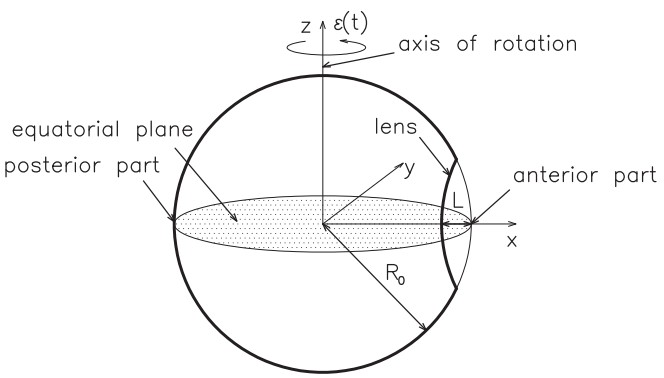

FIG. 1. Sketch of the domain under investigation.

TABLE I. Parameters and planes of measurement used for the experiments.

Expt. series	No. of runs	A (rad)	α	δ	Plane of measurement
s1–s28	305	0.07–0.35	2.5–50.4	0.1–0.3	Equatorial
s29–s31	36	0.174	3.5–17.6	0.1–0.3	Vertical

the amplitude of the saccades required to read was about 0.16 rad with a corresponding angular frequency ω around 50–60 s^{-1}. Therefore, using the typical dimension of the human eye and different values for the effective vitreous viscosity (healthy vitreous or liquefied vitreous) it is easy to show that in the case of reading movements the corresponding Womersley number may vary from about 3 to 40.

In the present analysis, we have employed a magnified physical model of the eye with a scale ratio of about 4. Therefore, scale effects need to be properly accounted for. In order to ensure similitude between the model and the prototype, we need to preserve all dimensionless parameters that matter for the problem. The parameters A and δ are preserved by rotating the eye model with the same amplitude as in real eye movements and scaling up the vitreous chamber geometry. Conservation of the dimensionless parameter α implies that the frequency of the eye movements shall be scaled accordingly.

The measurements were performed with the parameter values and planes of measurement shown in Table I. The three-dimensional flow (as well as the flow on the equatorial plane) is time dependent. In our analysis, we focus on the steady-streaming component of the flow on the equatorial plane, which is not time dependent. Note that the dynamics on the equatorial plane is not incompressible, i.e., the vertical (along the z axis) component of the velocity is identically zero but its derivative with respect to z is not. This has important implications for the transport barriers. The experiments cover a fairly wide range of the physical parameters; in fact, the Womersley number ranges from about 2 to a value of approximately 50, the oscillation amplitude was varied in the range [0.07,0.35] rad, which contains the most common physiological values, excluding microsaccades, and the indentation size is varied between 0.1 and 0.3.

Finally, note that in order to directly measure the steady streaming and filter out the oscillatory component of the flow with the 2D PIV system adopted, we set the pulse separation for image pairing, i.e., the time interval between two successive frames, to be a multiple of the oscillation period T.

III. METHODS

On the equatorial plane, starting from the Eulerian fields, Lagrangian particle trajectories can be numerically computed by integrating the equations:

$$\dot{\boldsymbol{x}} = \boldsymbol{f}(\boldsymbol{x}), \tag{1}$$

where $\boldsymbol{x}(t)$ is the particle position at time t and $\boldsymbol{f}(\boldsymbol{x})$ is the velocity field at point $\boldsymbol{x}$, starting from a uniform grid of initial conditions. In a 2D system with time-independent and a not-incompressible velocity field, we cannot have chaos or Kolmogorov-Arnold-Moser tori. Moreover, due to

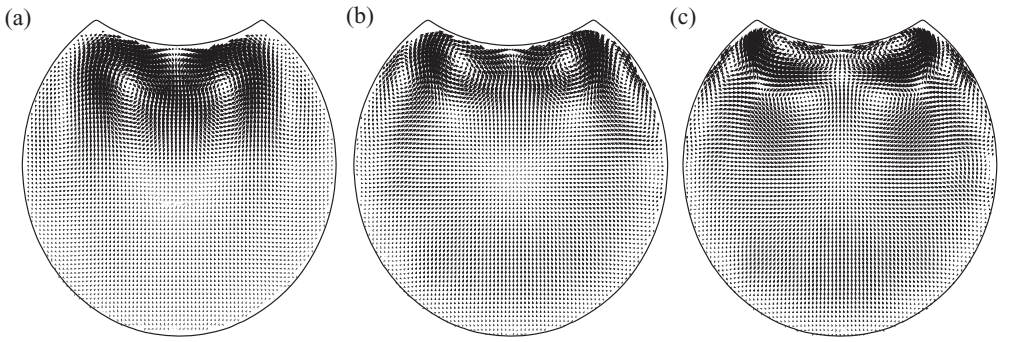

FIG. 2. Measured 2D velocity fields for $A = 0.0873$ rad, $\delta = 0.3$, and $\alpha = 12.06$ (a); $\alpha = 23.55$ (b); and $\alpha = 29.37$ (c).

the Poincaré-Bendixson theorem [17], the (complete) barriers to transport are limit cycles (either attracting or repelling periodic orbits) and multiple closed heteroclinic connections, whereas stable and unstable manifolds of saddle points are partial barriers to transport. Since we are analyzing only the steady-streaming component of the flow, we can detect these manifolds by numerically integrating the system forward and backward in time, starting from initial conditions very close to each saddle point.

Figure 2 shows three examples of velocity fields on the equatorial plane taken for different values of the Womersley number α, keeping the oscillation amplitude and indentation size fixed. For any value of the Womersley number the flow is dominated by the presence of intense circulation structures located in the anterior part of the domain close to the lens, whereas the posterior part seems not to be affected by the presence of the lens. In this region the flow is mainly radial toward the center of the domain as in the case of the steady streaming observed in a perfect sphere [6]. Increasing α, at fixed oscillation amplitude and geometry, several changes in the Eulerian fields can be observed, which lead to the appearance of different recirculations with different sense of rotation.

Since we intend to investigate the LCSs associated to the Eulerian fields, the starting point of our analysis are the Lagrangian trajectories, solutions of the dynamical system (1). We analyzed several system configurations by varying the three parameters (A, δ, and α) and we found that the dynamics of the system and therefore the location of the LCSs are mainly influenced by the Womersley number. This parameter is responsible for important bifurcations in the dynamical system.

IV. ANALYSIS

Figures 3 and 4 show results corresponding to some values of α. The saddle points are plotted as empty red circles and the other equilibrium points as green dots (if stable) or red crosses (if unstable). The dashed green and solid red curves are respectively the stable and unstable manifolds of the saddles, while the light gray ones are some trajectories of the drug particles. By looking at the stability of the equilibria and of the manifolds, it is straightforward to understand the direction of the particles. All the results have been obtained by considering an oscillation amplitude $A = 0.0873$ rad and an indentation $\delta = 0.3$.

The equilibrium points have been numerically located by finding the minima of the squared Euclidean norm of the velocity field by focusing on the equatorial plane regions where this function ranges between 0 and an upper limit. In our case, this limit is fixed as 1% of the maximum of the squared Euclidean norm over the whole domain. The stability properties of the detected points have been analyzed by evaluating the eigenvalues of the Jacobian matrix numerically computed in these points.

At low Womersley number [$\alpha = 12.06$; see Fig. 3(a)] all the drug particles on the equatorial plane are attracted by the two stable foci on the anterior part. Being the fluid incompressible, such foci must repel the mass particles along a direction which is transverse to the equatorial plane, i.e., considering the full 3D motion, the equilibria must be saddle foci. Similarly, the two unstable foci close to the boundary must attract trajectories along a direction transverse to the plane. We can notice that there is a separation between the left and right sides of the

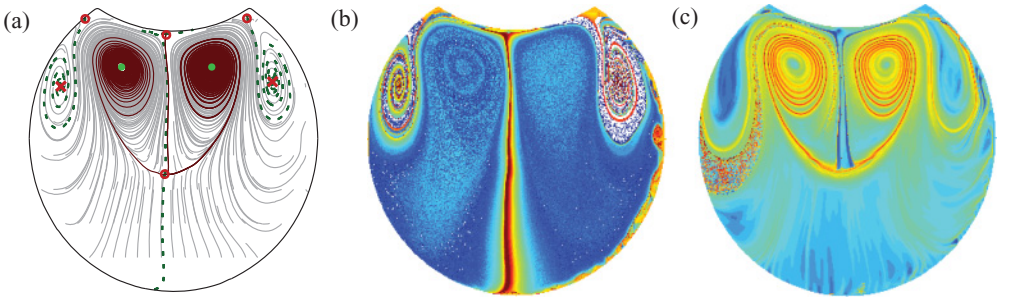

FIG. 3. (Color online) Streamlines obtained on the equatorial plane for $\alpha = 12.06$ (a) and corresponding forward (b) and backward (c) FTLEs fields.

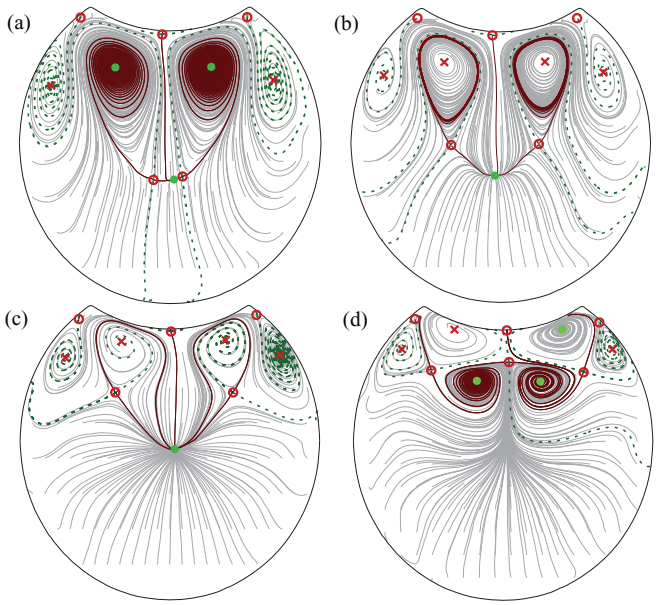

FIG. 4. (Color online) Streamlines obtained on the equatorial plane for $\alpha = 12.63$ (a), $\alpha = 15.58$ (b), $\alpha = 23.55$ (c), and $\alpha = 29.37$ (d) at fixed $A = 0.0873$ rad and $\delta = 0.3$.

plane and the separatrix is the stable manifold of the central saddle point. Such a manifold, in the anterior part of the eye, coincides almost exactly (there is a negligible difference due to measure and numerical errors) with the unstable manifold of the anterior saddle point, forming a heteroclinic orbit. The stable manifold of this point and also the unstable manifolds of the other two saddle points in the anterior part are on the boundary of the domain, where the measures of the vector field are less accurate. This situation remains the same for all the considered parameter configurations. For comparison, the same figure shows also the fields of finite-time Lyapunov exponents (FTLEs) $\sigma^{t_f}(\boldsymbol{x})$, obtained by forward-time [Fig. 4(b)] and backward-time [Fig. 4(c)] integrating system (1) according to the following definition [18]:

$$\sigma^{t_f}(\boldsymbol{x}) = \frac{1}{|t_f|} \ln \sqrt{\lambda_{\max}(\Delta)}, \tag{2}$$

where t_f is the integration time and $\lambda_{\max}(\Delta)$ is the largest eigenvalue of matrix

$$\Delta(\boldsymbol{x}) = J^T(\boldsymbol{x}) J(\boldsymbol{x}), \tag{3}$$

where $J(\boldsymbol{x})$ is the Jacobian matrix of the numerically computed flow map. The interested reader is referred to Ref. [18] for further details.

In Figs. 4(b) and 4(c), low FTLE values are represented in blue (light tones of gray), whereas high FTLE values are represented in red (dark gray). The latter evidence the presence of ridges in the scalar FTLE field, corresponding to the stable [Fig. 4(b)] and unstable [Fig. 4(c)] manifolds of the saddle points. It is evident that [Fig. 4(a)] summarizes the information of both Figs. 4(b) and 4(c).

An increase of the Womersley number to $\alpha = 12.63$ does not affect the dynamics of mixing within the eye in the anterior part [see Fig. 4(a)]. In the central part, on the contrary, we can notice that the saddle point undergoes a *pitchfork* bifurcation, thus becoming a stable point and originating two new saddle points around it. In this new situation it is no longer true that all the drug particles lying on the equatorial plane wrap around the stable foci: Some of them are attracted in the middle by this new stable node. Obviously, this equilibrium point must be a saddle-node for the complete 3D motion.

In [Fig. 4(b)] we show the streamlines for $\alpha = 15.58$. In this case all changes happen in the anterior part, where the stable foci become unstable through a supercritical *Hopf* bifurcation and two stable periodic orbits appear around them: the (solid red) unstable manifolds of the central saddle points overlap the stable periodic orbits. These periodic orbits define two closed regions in the plane, which trap particles inside them. We remark that the periodic orbits are very close to the stable manifolds of the central saddle points; by further increasing the Womersley number, the periodic orbits collide with the manifolds, thus inducing a *homoclinic* bifurcation which leads to the destruction of the periodic orbits [Fig. 4(c)]. In this situation all the drug particles in the equatorial plane are attracted by the central stable node (all other equilibria are unstable) and there is a separation between the anterior and the posterior parts of the plane.

A further increase of α leads to the result shown in Fig. 4(d). The two central saddle points move toward the anterior part and the stable node disappears. Moreover, a new saddle point and two stable foci are generated in the anterior part. In this region of the plane we can see four distinct closed regions in which the drug particles (lying on the plane) are trapped, while all the particles which are in the posterior region are attracted by the two new stable foci. This situation is similar to the first one we described, with the stable manifold separating the left and right side of the plane (the manifold changes direction near the center due to measure and numerical errors); the main difference is that the sense of rotation of the particles around the foci is opposite with respect to the previous situation with low Womersley number.

Note that if we change the values of A and δ and vary again the Womersley number, we obtain the same sequence of bifurcations but for slightly different α values. For instance, if we decrease the eye indentation, by keeping the oscillation amplitude fixed, the system undergoes the bifurcations at lower values of the Womersley number.

V. DISCUSSION

Although we considered a fairly simplified description of the eye movements, our analysis reveals interesting dynamics in the equatorial plane. The presented results are relevant in their own right and do not require a full 3D analysis in order to validate their importance. Moreover, they allow some preliminary considerations on the complete 3D dynamics; in the 3D domain, barriers will be surfaces whose intersections with the equatorial plane are the curves shown in the previous figures. Moreover, other barriers and more complex structures could be present. The first development of this work will concern the analysis of the 3D dynamics in this simplified model; then, more realistic scenarios (viscoelastic fluid, more complicated eye movements) will be considered. However, by combining the measurements on the equatorial plane with the ones on the vertical plane, it is already possible to get some

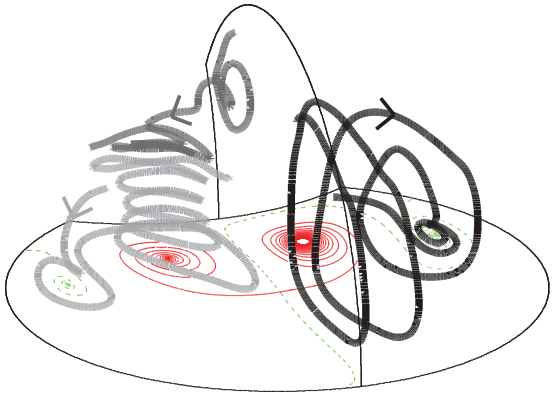

FIG. 5. (Color online) Some 3D trajectories for $\alpha = 12.06$.

insights about the 3D dynamics. An example of 3D trajectories obtained from an experimentally measured 3D velocity field is shown in Fig. 5 for a value of α close to 12.06 [see Fig. 3(a) for comparison of the trajectories on the equatorial plane]. Three trajectories are shown (with three different gray tones) in the upper half of the eye model. In the left sector two trajectories are plotted, which describe a vortex above one of the two saddle foci on the corresponding half of the equatorial plane. The presence of two further saddle foci can be guessed, one on the vertical plane (indeed we detected it in the 2D measurements on the vertical plane for similar parameter configurations) and one with unstable manifold between the two trajectories. In the right sector a trajectory is plotted, which initially shrinks around the stable manifold of a saddle focus on the equatorial plane and eventually tends to the unstable manifold of the same equilibrium. These samples, even if insufficient to get a complete idea of the dynamics within the eye, are consistent with the streamlines on the analyzed 2D sections and evidence the possible presence of complex behaviors.

VI. CONCLUSIONS

In this article, we have applied tools for the analysis of nonlinear dynamical systems to detailed experimental data sets reproducing a process of great importance for the treatment of common eye diseases. The existence of Lagrangian material structures might influence the success of these treatments, interfering with the delivery of drugs, and they have to be considered in order to optimize the position of commonly used release devices [3]. In particular, intravitreal delivery through direct injection of the drugs is one of the most used techniques of eye diseases treatment. Direct injections are usually performed through the transplana pathway (anterior part of the eye) and the drug is released 2–3 mm from the retina inside the vitreous chamber. In this case the drug is initially confined in a small volume in the anterior part of the vitreous chamber close to the lens. Note that very often the target of the treatment are segments of the retina located in the posterior half of the vitreous chamber, where retina breaks or detachments are most commonly observed. The presented results suggest that the anterior part of the chamber is dominated by the presence of Lagrangian structures that might confine mass (drug) in this part of the domain preventing its transport toward the posterior segment of the vitreous chamber.

The experiments discussed cover a wide range of parameters that represent many real eye movements (e.g., saccades and reading). In all cases the measured Eulerian flow fields have been found to be laminar. Turbulence is very unlikely to be generated for realistic values of the physical parameters (amplitude and Womersley numbers). In fact, only in the case of microsaccades the angular frequency can assume very high values, up to 10^3–10^4 s^{-1} (corresponding to high values of the Womersley number), but in this case the oscillation amplitudes are extremely small, leading to relatively small velocities in the vitreous body.

Finally, the methodology of Lagrangian analysis of experimental data here adopted represents an innovative and powerful approach to a variety of biomedical research problems.

ACKNOWLEDGMENTS

We are grateful to Professor Stephen Wiggins for discussions and comments on an earlier version of this manuscript.

[1] H. Lund-Andersen, in *Adler's Physiology of the Eye*, edited by P. L. Kaufman and A. Alm (Mosby, New York, 2003), 10th ed.
[2] W. Becker, in *The eurobiology of Saccadic Eye Movements*, edited by R. Wurtz and M. Goldberg (Elsevier Science, Amsterdam, 1989).
[3] D. Maurice, J. Ocul. Pharmacol. **17**, 393 (2001).
[4] S. C. Pflugfelder, E. Hernandez, S. J. Fliesler, J. Alvarez, M. E. Pflugfelder, and R. K. Forster, Arch. Ophthalmol. **105**, 831 (1987).
[5] C. R. Ethier, M. Johnson, and J. Ruberti, Annu. Rev. Biomed. Eng **6**, 249 (2004).
[6] R. Repetto, J. H. Siggers, and A. Stocchino, J. Fluid Mech. **608**, 71 (2008).
[7] A. Stocchino, R. Repetto, and J. H. Siggers, Phys. Med. Biol. **55**, 453 (2010).
[8] G. Boffetta, G. Lacorata, G. Redaelli, and A. Vulpiani, Physica D **159**, 58 (2001).
[9] G. Haller and G. Yuan, Physica D **147**, 352 (2000).
[10] G. Lapeyre, Chaos **12**, 688 (2002).
[11] F. d'Ovidio, V. Fernandez, E. Hernandez-Garcia, and C. Lopez, Geophys. Res. Lett. **31**, L17203 (2004).
[12] S. Wiggins, Annu. Rev. Fluid Mech. **37**, 295 (2005).
[13] S. Shadden, J. Dabiri, and J. Marsden, Phys. Fluids **18** (2006).
[14] M. Mathur, G. Haller, T. Peacock, J. E. Ruppert-Felsot, and H. L. Swinney, Phys. Rev. Lett. **98**, 144502 (2007).
[15] S. P. Liversedge and J. M. Findlay, Trends Cogn. Sci. **4**, 6 (2000).
[16] S.-N. Yang and G. W. McConkie, Vision Res. **41**, 3567 (2001).
[17] S. Wiggins, *Introduction to Applied Nonlinear Dynamical Systems and Chaos*, 2nd ed. (Springer, New York, 2003).
[18] S. Shadden, F. Lekien, and J. Marsden, Physica D **212**, 271 (2005).